Available online at www.sciencedirect.com
SCIENCE DIRECT
Polymer 46 (2005) 2943–2949
polymer
www.elsevier.com/locate/polymer

Confocal Raman study of poly(ethylene terephthalate) fibres dyed in supercritical carbon dioxide: dye diffusion and polymer morphology

O.S. Fleming[a], S.G. Kazarian[a,*], E. Bach[b], E. Schollmeyer[b]

[a]*Department of Chemical Engineering and Chemical Technology, Imperial College London, London SW7 2BY, UK*
[b]*German Textile Research Centre, North-West e.V., Krefeld, Germany*

Received 15 May 2004; received in revised form 5 December 2004; accepted 7 February 2005
Available online 11 March 2005

Abstract

Confocal Raman microscopy (CRM) has been used to extract dye diffusion data from poly(ethylene terephthalate) (PET) fibres dyed with Disperse Yellow 23 under supercritical CO_2 conditions. Spectral information as a function of depth was measured in a non-destructive manner using dry and oil objectives in confocal Raman mode. Mapping along the radius of the fibre cross-section was performed and compared to the data from the confocal measurements. A significant dye concentration gradient has been observed along the line normal to the fibre surface which the data from the oil confocal measurements accurately describes to a depth of 45 μm. The effect of the supercritical CO_2 dyeing process on the fibre morphology has also been evaluated using CRM.

Keywords: Polymer dyeing; Crystallinity; Depth profile

1. Introduction

The use of supercritical (sc) CO_2 technology as a replacement for the traditional aqueous method for dyeing of poly(ethylene terephthalate) (PET) is a commercially viable alternative that has grown in international interest since 1995 [1]. In polymer processing terms, $scCO_2$ can be considered as 'solvent-free' plasticising agent as under normal conditions CO_2 is a gas and therefore there is no residual solvent in the material following processing. Furthermore, the degree of swelling in the polymeric matrix can be 'tuned' by adjusting the pressure of the system and thus the mass transfer within the polymer may be controlled [2]. These properties make the use of $scCO_2$ attractive for the impregnation of amorphous and semi-crystalline polymers with doping solutes in an essentially solvent-free manner [3–5]. In cases where the desired impregnation dye has a low solubility in the CO_2 phase, the affinity of the dye to the polymer results in partitioning between the two phases and consequently successful impregnation is possible [2]. The inexpensive, non-toxic, non-flammable and environmentally benign nature of CO_2 is an obvious driver for the replacement of traditional solvents in polymeric material processing. In the case of the dyeing industry, the implementation of $scCO_2$ technology over the traditional aqueous method would result in a great gain in the rate of diffusion [6] and would offer further benefits by reducing the number of effluent streams and allowing the location of industry to areas where water supplies are limited [7].

Optimisation of the $scCO_2$ dyeing process requires knowledge of the dye mass transport through the polymer matrix. Methods used to investigate the $scCO_2$ dyeing of polymers include the film roll method [6,8] and the gravimetric approach [9]. Table 1 summarises the diffusion coefficients for Disperse dye/PET systems calculated by various experimental techniques. Measuring the total dye uptake is limited in the sense that it does not reveal the spatial distribution of dye through the film thickness. Confocal Raman microscopy (CRM) is a technique that is particularly suited to investigating such distributions within polymers, as spectral information is recorded as a function of depth within the sample, and hence the diffusion mechanism of the dye may be evaluated. We have demonstrated the feasibility of CRM to investigate the dye

* Corresponding author.
E-mail address: s.kazarian@imperial.ac.uk (S.G. Kazarian).

0032-3861/$ - see front matter © 2005 Elsevier Ltd. All rights reserved.
doi:10.1016/j.polymer.2005.02.067

Table 1
Summary of dye diffusion analysis on PET/Disperse dye systems

Temperature (°C)	Pressure (bar)	Geometry	Dye	Measurement technique	D (m^2s^{-1})	Ref.
120	300	Cylindrical fibre (1.3 mm (∅)	C.I Disperse Red 324	Gravimetric	1.07×10^{-13}	[9]
120	300	Cylindrical fibre (1.3 mm (∅)	C.I. Disperse Orange 149	Gravimetric	1.93×10^{-11}	[9]
90	220	Cylindrical film roll-(effectively 6 mm ∅)	Disperse Yellow	Film roll method combined with UV–vis	1.4×10^{-14}	[8]
90	220	Cylindrical film roll-(effectively 6 mm ∅)	Disperse Blue	Film roll method combined with UV–vis	2.3×10^{-14}	[8]
110	220	Cylindrical film roll-(effectively 6 mm ∅)	Disperse Yellow	Film roll method combined with UV–vis	1.2×10^{-13}	[8]
110	220	Cylindrical film roll-(effectively 6 mm ∅)	Disperse Blue	Film roll method combined with UV–vis	1.1×10^{-13}	[8]
110	250	Cylindrical film roll-(effectively 6 mm ∅)	Disperse Yellow	Film roll method combined with UV–vis	1.5×10^{-13}	[8]
110	250	Cylindrical film roll-(effectively 6 mm ∅)	Disperse Blue	Film roll method combined with UV–vis	1.6×10^{-13}	[8]
120	250	Cylindrical film roll	C.I. Disperse Red 324	Film roll method combined with UV–vis	7.1×10^{-14}	[6]
100	250	Cylindrical film roll	C.I. Disperse Red 324	Film roll method combined with UV–vis	1.2×10^{-14}	[6]
100	200	Cylindrical film roll	C.I. Disperse Red 324	Film roll method combined with UV–vis	9.0×10^{-15}	[6]
100	150	Cylindrical film roll	C.I. Disperse Red 324	Film roll method combined with UV–vis	2.4×10^{-15}	[6]
100	150	Cylindrical film roll	C.I. Disperse Red 324	Film roll method combined with UV–vis	7.1×10^{-14}/10% Ethanol modifier	[6]
100	170	Cylindrical film roll	C.I. Disperse Red 324	Film roll method combined with UV–vis	5.5×10^{-14}/8.5% Ethanol modifier	[6]

concentration distribution in PET film processed with $scCO_2$ [10] and more recently (combined with FTIR imaging) revealed a morphological gradient induced by $scCO_2$ exposure [11,12].

CRM traditionally uses a dry, metallurgical objective to focus the laser light into the sample and to collect the backscattered light. However, interpretation of the Raman depth profile data is complicated by refraction effects occurring at the air/sample interface. Optical aberrations to the focal volume as a result of refraction [13–16] lead to the uncertainty of the *z*-position of the laser focus within the sample (light is refracted deeper in the sample than the distance that the sample has moved relative to the objective) and an increase in the point spread function of the focal volume. The ability to obtain pure spectra within the sample is lost due to 'spectral leakage' within the enlarged focal volume. The use of an oil immersion objective (combined with an immersion oil of similar refractive index as the sample being studied) improves the refractive index mismatch and consequently an improvement in the depth resolution is possible [15,17]. The implementation of an immersion oil objective has realised the power of CRM to study polymeric materials [10,17]. CRM has also been applied (in situ) to study diffusion of penetrant species through a membrane [18] and the diffusion in multi-component liquid systems [19].

In this work, CRM has been applied to polymeric fibres dyed under $scCO_2$ conditions of which are of specific interest to the textile industry. PET monofilaments are well suited to investigate dye distribution in polymers due to their yarn size. While PET multifilament yarn is completely dyed very easily, fiber cross-sections of monofilaments with a bigger diameter show ring dyeing effects in water as well as in $scCO_2$ also after dyeing times of up to 6 h at 130 °C

[20]. If PET monofilaments have to be coloured completely, a spin mass dyeing process has to be carried out which is much more inflexible compared to water dyeing, more expensive at short yardage, and needs high dye concentrations [21]. Typical applications of the PET monofilaments used in this study are textile accessories such as zippers and velcro fastenings. The first dyeing results of such products from PA 6.6 in $scCO_2$ have already been published by Knittel et. al. [22] in 1993 but lacked details of dye distribution within the fibres. In this context, fibres dyed on a laboratory scale for different periods of time have been investigated and the diffusion coefficient of the dye within the polymer has been determined. The consequence of the dyeing process on the fibre morphology has also been evaluated because changes in the crystallinity during dyeing can highly influence the dye uptake of synthetic fibres and the diffusion coefficient of the dye in the polymer matrix [23].

2. Experimental

Poly(ethylene terephthalate) (PET) monofilament fibres (Trevira® Monofil 900 S, Trevira, Bobingen, Germany) with a diameter of 0.4 mm were treated in $scCO_2$ with and without C.I. Disperse Yellow 23 (DY23) from Ciba Specialty Chemicals, Basle Switzerland at a dye concentration of 5% relating to the fabric weight for 1, 2 and 3 h. The fibres (1.8 g (approx. 10 m), relating to a weight to volume ratio of w/v 1:222) were placed in a stirrable perforated dyeing beam within a 400 ml high pressure apparatus as described elsewhere [22]. The dye was filled into an aluminum tin covered with filter paper and placed at the bottom of the autoclave. The autoclave was filled with gaseous CO_2 at 45 bar and heated up to 130 °C. To avoid dissolution of the dye as far as possible during the heating phase the pressure was raised to 280 bar only when the treatment temperature was reached. 50 x objectives (oil and dry) were used to measure all of the Raman spectra in this work. The immersion oil used in combination with the immersion objective had a refractive index of 1.515 (purchased from Cargille Laboratories Inc, Cedar Grove, NJ).

All Raman spectra were recorded with a dispersive Renishaw 1000 confocal system using the 785 nm line of a solid diode laser. A two-dimensional Peltier cooled charge-coupled device (CCD) camera was used to record the 180° backscattered Raman light. Confocal performance was achieved by closing the slit width in the spectrometer to approximately 15 μm and the pixel binning of the CCD limited to 4 pixels to form a 'synthetic' confocal aperture. The depth profiles presented in this work were generated by recording Raman spectra at 1 μm increments along the line normal to the surface of the fibre. The collection process was automated with a motorised xyz stage and controlled with a computer. The depth resolution of a confocal Raman microscope can be determined from the FWHM (full width at half maximum) of the 520 cm^{-1} response curve from a *z*-sectioned silicon wafer. In confocal mode we achieve a depth resolution of ca. 4 μm with a nominal spectral resolution of 1 cm^{-1}/pixel. It should be noted that the depth resolution will be degraded upon focusing the laser below the surface of a transparent film, due to refraction effects at the surface boundary as previously described.

The Raman spectroscopic analysis was performed in a three part process in order to assess the feasibility of the non-destructive technique:

1. Dry Confocal: Raman spectra were recorded at 1 μm increments along the line normal to the fibre surface using a traditional dry, metallurgical objective.
2. Oil Confocal: Raman spectra were recorded at 1 μm increments along the line normal to the fibre surface using an oil immersion objective with an immersion oil filling the optical path between the lens and the material.
3. Conventional Raman line mapping: the fibre was microtomed at the central position to allow lateral line mapping to be performed along the radius of the cross-section. The high spatial resolution available with this method (ca. 1–2 μm) serves as reference data to compare the confocal data generated in the dry and oil approaches.

The thermal analyses of PET before and after treatment in $scCO_2$ were carried out on a TA Instruments calorimeter DSC 2910 (Alzenau, Germany). The temperature range of the thermograms was between 20 and 300 °C with a heating rate of 10 or 20 °C/min. Temperature calibration of the DSC cell was carried out by measuring the melting points of Gallium, Indium, and Tin within an accuracy of ± 0.01 °C. Calibration of the enthalpy with Indium was within an accuracy of 0.41 J/g.

3. Results and discussion

3.1. Surface analysis

Raman spectra were collected in confocal mode to limit the amount of material probed by the focal volume to the top few micrometers of the sample. All fibres were aligned parallel to the longest dimension of the line laser, and the measurement position (central point along the radius of the fibre) located using the visible microscope and the motorised stage. Our method of analysis allows us (with the use of an internal standard for signal normalisation) to assess the concentration of the impregnated dye and the intrinsic morphology of the guest polymer matrix. We have recently demonstrated that confocal Raman microscopy can be used to probe the subtle features of semi-crystalline PET processed with $scCO_2$ with induced crystallinity evaluated from the narrowing of the carbonyl band as a result of the formation of the planer crystalline structure [12].

Raman spectra corresponding to the fingerprint region of a selection of the fibres anlaysed in this study are shown in Fig. 1. Representative spectra of the unprocessed fibre and fibres exposed at 280 bar and 130 °C for 3 h in the absence (B) and presence (C) of DY23 are presented. Spectrum D corresponds to pure DY23 generated via spectral subtraction of B from C. The chemical structure of Disperse Yellow 23 can be seen in Fig. 2 and the associated strong Raman activity of the dye can be seen in the spectral region of 1360–1500 cm^{-1}. The Raman signal originating from the dye is proportional to the concentration and thus the spectra may be used to study the relative concentration of which was assessed by the integrated area of the wavenumber range 1454–1475 cm^{-1}.

The spectrum of the unprocessed fibre (A) shown in Fig. 1 is characteristic of PET with a relatively high degree of crystallinity. This may be interpreted from the spectral regions of the carbonyl band, the shoulder at 1096 cm^{-1} and the band at 1000 cm^{-1}. The band at 1000 cm^{-1} corresponds to the trans conformation of the glycol unit and is indicative of the crystalline morphology (the gauche conformation is inherent to the amorphous domains of PET). The band at 1117 cm^{-1} has a shoulder at 1096 cm^{-1} that corresponds to the combination stretching vibration of the ester, glycol and ring unit of the trans configuration of the PET chain. However, the presence of both of the aforementioned observations can occur in domains of amorphous PET that lack three-dimensional order. The true crystallinity indicator of PET is the narrowing of the carbonyl band as a result of the planarity existing between the carbonyl group and ring system [24]. The ability of CO_2 to plasticize amorphous domains in PET has the consequence of the necessity to consider induced morphological alterations during processing. Dissolved CO_2 molecules interact with the basic sites along the polymer, reduce the non-specific chain–chain interactions, and enhance the

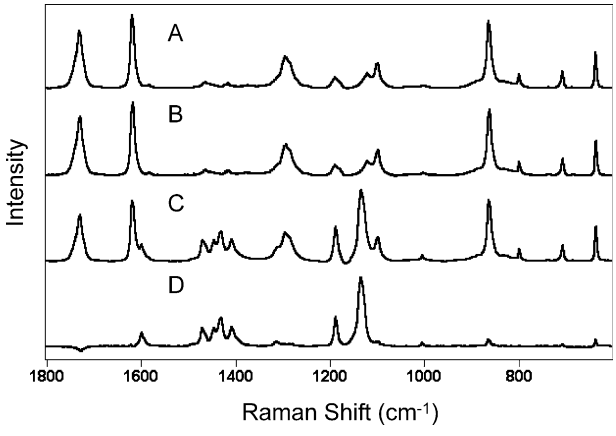

Fig. 1. Raman spectra (acquired with a 50× dry objective in confocal mode) measured at the surface of the 0.4 mm fibres. Spectrum A corresponds to the unprocessed fibre and spectra B and C following 3 h exposure to $scCO_2$ at 280 bar and 130 °C in the absence and presence of Disperse Yellow 23, respectively. Spectral subtraction of B from C was used to generate spectrum D which corresponds to Disperse Yellow 23.

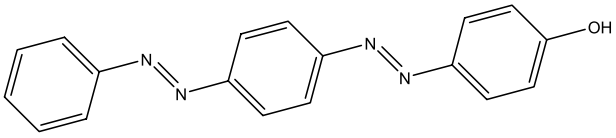

Fig. 2. Chemical structure of Disperse Yellow 23.

segmental mobility of the chains [25]. The imposed mobility of the chains allows them to reorganise into the lowest energy configuration, which happens to be the planer crystalline form [26]. Upon depressurisation the CO_2 quickly escapes in the form of gas, and the induced morphology is frozen.

The carbonyl band of the unprocessed fibre has a FWHM value of 18 cm^{-1} which compared to the amorphous form (ca. 27 cm^{-1}) corresponds to semi-crystalline PET with a relatively high degree of crystallinity. Following 3 h exposure to $scCO_2$ at 280 bar and 130 °C (spectrum B) there are no changes to the spectral features associated with crystallinity. The effect of the CO_2 dyeing process on the crystallinity of the polymer has been evaluated in terms of the narrowing of the carbonyl band compared to the unprocessed fibre. The width of the carbonyl band does not significantly narrow for any of the dyeing times investigated which reflects that the $scCO_2$ processing does not lead to any increase in crystallinity at the fibre surface and provides evidence for the applicability of the carbonyl band to be used for dye concentration normalization, as described later. Additionally, DSC measurements were carried out to detect structural changes in the PET caused by the treatment in $scCO_2$. First of all, the DSC-curves of the untreated PET show two endothermic peaks, a very small one with a melting enthalpy of approx. 1.2 J/g between 170 and 200 °C with a maximum at 185 °C and the melting peak of PET at 256 °C. The pre-melting peak correlates to the so called effective temperature which indicates, according to Berndt et al. [27], that the fibre has been heat set at 185 °C before $scCO_2$ dyeing. This process is carried out in the textile industry to avoid changes in the crystallinity of the semi-crystalline polymer during dyeing in water as well as in $scCO_2$ [22,23,27]. Heat setting was proved by heating the untreated PET monofilament in a DSC-cell up to the heat set temperature of 185 °C at a rate of 10 and 20 °C/min, cooling down the cell rapidly to 20 °C with ice and heating up once again above the melting point of PET. After the second heating the melting enthalpy of the pre-melting peak increased to 2.8 J/g at a heating rate of 20 °C/min starting at 166 °C up to 203 °C with a maximum at 196 °C and to 4.1 J/g at 10 °C/min starting at 144 °C up to 203 °C with a maximum at 188 °C. In the latter experiment the pre-melting peak was broadened due to the lower temperature gradient. These results indicate that the crystallization processes in the semi crystalline regions of the PET occurred during the first heating showing that heat setting of the monofilament fiber was incomplete. This means that crystallization can also possibly occur during treatment of

PET in $scCO_2$. As seen in the Raman spectra, the DSC measurements also do not show any differences in the DSC curves and the melting enthalpies of the pre-melting peak between the untreated, $scCO_2$-treated and dyed samples, even after a treatment for 6 h at 130 °C at 280 bar in $scCO_2$.

3.2. Depth profiling/z-sectioning

The dye concentration gradient in the polymer samples was investigated along the line normal to the fibre surface (z-direction) to enable an analysis of the dye concentration as a function of depth in the polymer. The suitability of CRM using an oil immersion objective to study depth profiles of such dye/polymer systems has previously been demonstrated by Kazarian and Chan [10]. Raman depth profiles of the fibre dyed for 3 h measured with both the oil and dry objectives are shown in Fig. 3(a) and (b). Spectra were collected at 1 μm increments along the line normal to the fibre surface and the measurement position was located using the optical microscope and the motorised stage. In both the dry and oil data it can be seen that the concentration of the dye is not uniform as a function of depth but decays in concentration from the surface to the core of the polymer, as seen with the decrease of the dye bands relative to that of the polymer. There are two main features that differ between the depth profiles of the oil and dry approaches; an underestimation of the extent of the dye gradient in the case of the dry method; and the decrease in intensity of all Raman bands with depth in the dry approach compared to the oil data. The Raman spectra from the dry data show a significant decay of the polymer bands over the initial 100 μm depth, whereas the oil data show a small drop in intensity over this range. The improvement in refractive index mismatch when employing the immersion objective results in the reduction of refraction at the sample surface and hence minimises the optical aberrations associated with the enlargement and distortion of the focal volume with depth. In the case of the dry metallurgical objective, the refraction of light at the air/surface boundary result in a situation whereby the distance that the stage is moved in the z-direction does not describe the actual depth of focus within the sample. The increase in the point spread function of the focal volume results in the lasing energy being spread over a large volume (relative to the ideal case in which the entire optical path contains no refractive index mismatches) and hence we observe a reduction in Raman intensity with depth.

However, to compare the two depth profiles it is necessary to account for possible laser power fluctuations, which was accomplished using band area normalisation. Dye band normalisation was performed by dividing its area by the area of the carbonyl band. The dye band was integrated over the wavenumber range 1454–1480 cm^{-1} and for the carbonyl band the range 1700–1760 cm^{-1} was used. Peak area measurements were performed using the original baseline and the area under the peak was integrated using a straight line that connects the aforementioned data points. The normalized intensity of the dye concentration gradient for the oil and dry confocal data is compared with the results obtained from the line mapping of a microtomed section of the same fibre in Fig. 4. The high spatial resolution available with conventional lateral mapping of

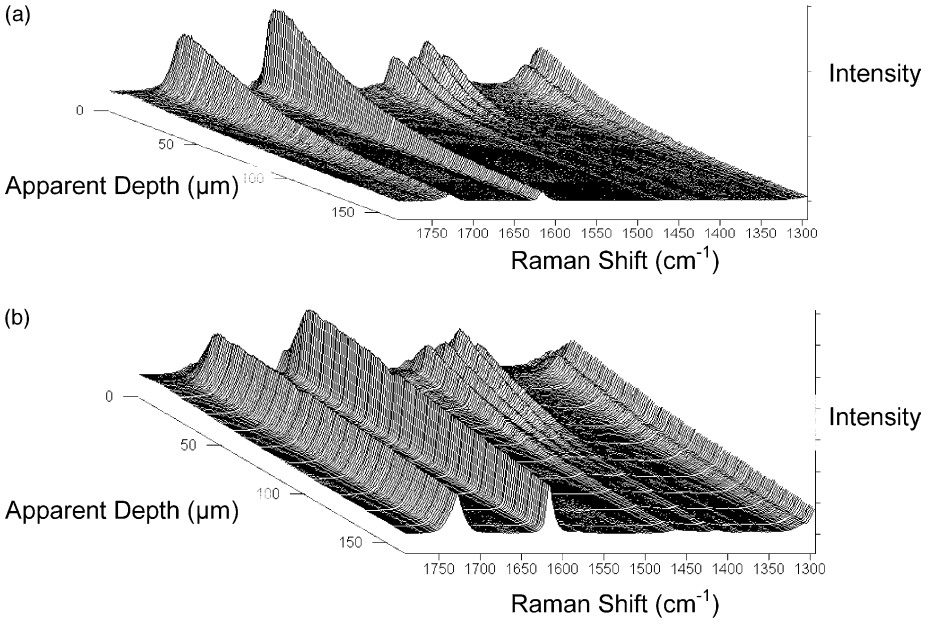

Fig. 3. (a) Confocal Raman depth profiles of the fibre dyed for 3 h collected with the 50× dry objective. Spectra were recorded at 1 μm increments along the line normal to the fibre surface. (b) Confocal Raman depth profiles of the fibre dyed for 3 h collected with the 50× oil objective. Spectra were recorded at 1 μm increments along the line normal to the fibre surface.

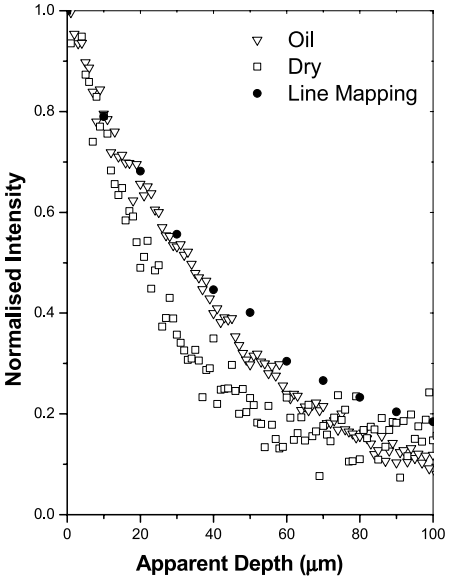

Fig. 4. Comparison of confocal (oil and dry) data with the line mapping results from a microtomed cross-section of the fibre.

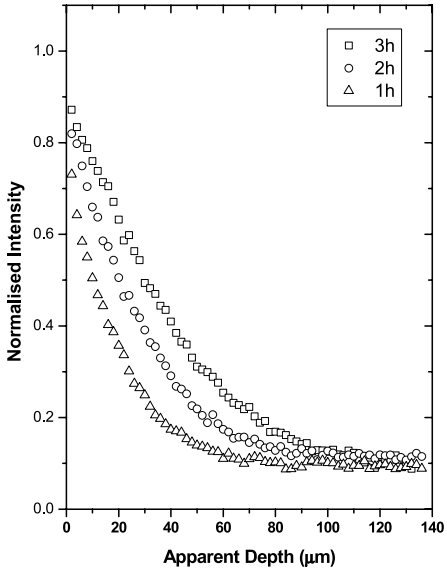

Fig. 5. Oil immersion dye concentration gradients; comparison of dyeing time.

the fibre is in the order of 1–2 μm, which gives us reference data of the dye distribution to compare the confocal data, and hence evaluate the confocality of the two methods. Over the initial 45 μm in the sample the oil confocal data reveal the same gradient as the line mapping data, compared to the dry confocal data of which underestimates the extent of the gradient by a factor of approximately 1.5. At depths greater than 45 μm the oil data deviates from the line mapping data and underestimates the concentration of dye at greater depths. Fig. 4 demonstrates the reliability of the oil confocal approach to probe relatively deep within such polymer systems and highlights the inaccuracies associated with the use of the traditional dry objective. As mentioned by Everall [17], if it is required to probe deeper within the sample it would be advisable to microtome the sample and hence take advantage of the high spatial resolution available when performing point mapping (operating at the diffraction limit of the laser).

The normalised dye concentration distributions as a function of depth for the polymer fibres, collected using the oil immersion objective, are shown in Fig. 5. The dye distribution gradients yield the change in concentration of the dye within the fibre as a function of time and using these data conclusions can be drawn on the diffusion characteristics of the dye in the polymer. A plot of the normalised dye fraction as a function of the square root of exposure time is shown in Fig. 6. The linear plot is characteristics of Fickian diffusion of which is expected as a result of the fast rate of polymer chain relaxation compared to the rate of dye diffusion. In this case the Fickian model describes one-dimensional diffusion of dye through a finite plate under the assumption of constant diffusion coefficient. The slope of the plot was used to estimate the dye diffusion coefficient of DY23 in the PET fibres at 3.5×10^{-13} m^2s^{-1}. This value compares well with literature data reported by Sicardi et al. [8] who applied UV–vis spectroscopy to a Disperse Yellow/PET system processed using the film roll method, reporting a diffusion coefficient of 1.5×10^{-13} m^2s^{-1}. However, due to the processing conditions (110 °C and 250 bar compared to 130 °C and 280 bar used in this work), the difference in experimental procedure (Film roll followed by UV–vis compared to non-invasive CRM) and the nature of the yellow dye may not have been the same as used in our study we are unable to directly compare the results.

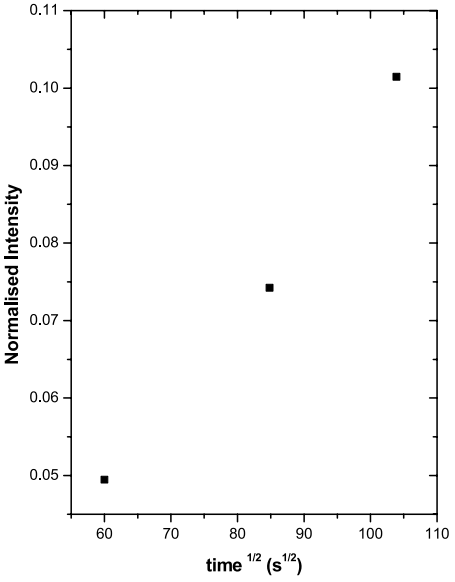

Fig. 6. Plot of the normalised intensity of dye fraction vs. the square root of exposure time.

4. Conclusions

Confocal Raman microscopy has been used to study, in a non-invasive manner, the dye concentration distribution as a function of depth in polymeric fibres dyed from a supercritical solution. A significant dye concentration gradient has been detected along the line normal to the fibre surface and studied as a function of dyeing time. An estimate of the dye diffusion coefficient has been calculated and the morphology of the fibre following processing evaluated. This study demonstrates the suitability of CRM in conjunction with an oil immersion objective to study such polymeric fibres and the disadvantages associated with the use of the dry objective. Information regarding the distribution of the guest dye molecules as well as the intrinsic morphology of the host polymer matrix makes the use of CRM a powerful technique for material characterisation of the dyed fibres.

Acknowledgements

We thank EPSRC (grant number GR/R57164/01) for financial support. We also thank Renishaw, plc for help and advice.

References

[1] Bach E, Cleve E, Schollmeyer E. Rev Prog Color 2002;32:88.
[2] West BL, Kazarian SG, Vincent MF, Brantley NH, Eckert CA. J Appl Polym Sci 1998;69:911.
[3] Cooper AI. J Mater Chem 2000;10:207.
[4] Kazarian SG. Polym Sci Ser C 2000;42:78.
[5] Tomasko DL, Li H, Liu D, Han X, Wingert MJ. Ind Eng Chem Res 2003;42:6431.
[6] Sicardi S, Manna L, Banchero M. Ind Eng Chem Res 2000;39:4707.
[7] Kazarian SG, Brantley NH, Eckert CA. CHEMTECH 1999;36.
[8] Sicardi S, Manna L, Banchero M. J Supercritcal Fluids 2000;17:187.
[9] Schnitzler J, Eggers R. J Supercritcal Fluids 1999;16:81.
[10] Kazarian SG, Chan KLA. Analyst 2003;128:499.
[11] Fleming OS, Chan KLA, Kazarian SG. Vib Spectrosc 2004;35:3.
[12] Fleming OS, Kazarian SG. Appl Spectrosc 2004;58:391.
[13] Vyor Ykka J, Halttunen M, Iiti H, Tenhunene J, Vuorinen T, Stenius P. Appl Spectrosc 2002;56:776.
[14] Reinecke H, Spells SJ, Sacristan J, Yarwood J, Mijangos C. Appl Spectrosc 2001;55:1660.
[15] Everall N. Appl Spectrosc 2000;54:773.
[16] Baldwin KJ, Batchelder DN. Appl Spectrosc 2001;55:517.
[17] Everall NJ. Appl Spectrosc 2000;54:1515.
[18] Schmiitt M, Leimeister B, Baia L, Weh B, Zimmermann I, Kiefer W, et al. CHEMPHYSCHEM 2003;296.
[19] Bardow A, Marquardt W. AIChe 2003;49:323.
[20] Bach E. Unpublished results.
[21] http://www.swicofil.com/setilawidnau/polyester_in_automotive-Dateien/polyesterinauto.doc
[22] Knittel D, Saus W, Schollmeyer E. J Text Inst 1993;84:534.
[23] Cleve E, Bach E, Schollmeyer E. Angew Makromol Chem 1998;256:39.
[24] Adar F, Noether H. Polymer 1985;26:1935.
[25] Kazarian SG, Vincent MF, Bright FV, Liotta CL, Eckert CA. J Am Chem Soc 1996;118:1729.
[26] Kazarian SG, Brantley NH, Eckert CA. Vib Spectrosc 1999;19:277.
[27] Berndt HJ, Bossmann A. Polymer 1976;17:241.